NANO LETTERS

Letter

pubs.acs.org/NanoLett

A Simple Self-Calibrating Method To Measure the Height of Fluorescent Molecules and Beads at Nanoscale Resolution

Jacob W. J. Kerssemakers,[†] Timothy R. Blosser,[†] and Cees Dekker*

Department of Bionanoscience, Kavli Institute of Nanoscience, Delft University of Technology, Lorentzweg 1, 2628 CJ Delft, The Netherlands

Supporting Information

ABSTRACT: We describe a simple self-calibrating technique, incident-beam interference sweeping, for measuring the height of fluorescent labels. Using a tilted back-reflecting mirror and a scanning laser beam, a modulated fluorescence emission allows height determination of a label from a surface with a resolution of ∼3 nm. In addition, we show that the absolute distance of a label from the top-mounted mirror can be determined with a resolution of a few tens of nanometers over a micrometer range.

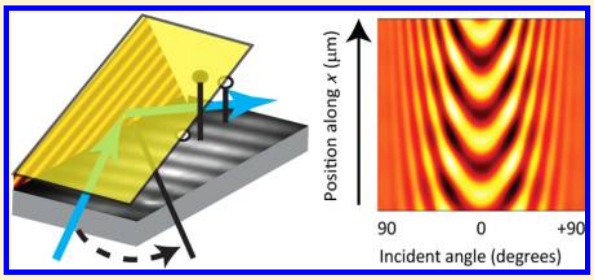

KEYWORDS: *Height determination, fluorescence, total internal reflection fluorescence, nanoscale resolution*

Many biological processes can only fully be understood if the full spatial configuration of contributing components, such as proteins or organelles, can be monitored at the nanometer scale. In recent years, fluorescent labeling of molecules has greatly advanced microscopy-based tracking, yielding nanoscale resolution within the imaged plane.

Numerous approaches exist for this lateral ("*x*,*y*") position determination of fluorescently labeled particles or molecules. However, because most biological processes are three-dimensional in nature, for full understanding it is important to be able to measure in three dimensions. Unfortunately, much fewer methods are available for determining position along the vertical optical axis ("*z*"). This is partly due to technical demands; while a single image acquired with any standard microscope suffices for (*x*,*y*)-tracking, measuring along the optical axis perpendicular to the imaging plane involves technical alterations. For example, under epi- or confocal illumination multiple images obtained at different heights, or "defocus stacks", require axial movement of the objective and offer limited resolution, although an engineered point spread function (PSF) involving cylindrical lenses recently showed some progress.[1,2] Specialized samples involving microfabricated mirror pits that image the axial position in the lateral plane have also been reported.[3] These approaches, however, have yet to demonstrate nanoscale resolution over the full field of view.

Higher resolutions were obtained by several height-measuring techniques that involve a static, axial height-dependent illumination pattern. The most commonly known are total internal reflection fluorescence (TIRF) microscopy, where an evanescent field penetrates up to ∼200 nm into a sample, and fluorescence interference contrast (FLIC) microscopy, where a reflecting surface causes a standing illumination pattern throughout a sample.[4−6] A number of studies involve the use of vertically modulated illumination patterns.

For example, enhanced axial resolution was reported with spatially modulated illumination (SMI) where a standing wave pattern was generated in a sample by either two objectives or by one objective and a back-reflecting mirror.[7,8] In general, the brightness of the fluorescence emission of a label in such a static illumination field contains height information. For example, in the case of TIRF the evanescent optical intensity explains the observation that the further a particle is from the sample surface, the dimmer it is. One drawback to any static illumination scheme is that two particles with different intrinsic brightnesses can exhibit different intensities at the same height, which can complicate or confound accurate height determination. Techniques based on static illumination patterns thus require careful calibration of light intensity and fluorophore properties, which may require rather elaborate microfabricated, stepped samples[5,9] or experiment-specific approaches.

The influence of the intrinsic brightness difference of labels can be diminished by using dynamic illumination schemes. In such a scheme, the illumination is varied such that a label experiences a range between minimum and maximum illumination. The relative modulation (phase) of the resulting fluorescence emission is height dependent and the intrinsic brightness of the label is only reflected in its amplitude. An example of such a dynamic modulation technique was reported involving the scanning of an interference pattern under an atomic force cantilever tip.[10] This technique showed very high, nanoscale resolution without the need for fluorescence calibration but involves the simultaneous use of an atomic

Received: April 17, 2014
Revised: June 13, 2014
Published: July 11, 2014

 © 2014 American Chemical Society dx.doi.org/10.1021/nl501434v | *Nano Lett.* 2014, 14, 4469−4475

force microscope scanning device and confocal fluorescent imaging, which is nontrivial to implement in most optical setups.[4] In recent years, fluorescent lifetime microscopy (FLIM) near metal surfaces was shown to allow high-resolution axial measurement independent of the intrinsic brightness of a label,[10,11] but this approach is not compatible with the more commonly used glass slide-based sample surfaces.

While a few existing techniques thus do provide nanoscale resolution, all of the techniques require either elaborate sample preparation by microfabrication, careful tuning of the illumination field, imaging of a tuned single-molecule PSF, or an elaborate combination of techniques.

Here, we introduce a nanoscale-precision height-measurement scheme called incident-beam interference sweeping (IBIS), which has a minimum of sample/setup requirements and which is based on dynamic illumination, such that label properties or emission strengths do not interfere with height determination.

Basic Setup of IBIS. An IBIS measurement is set up by two simple alterations of a standard TIRF microscope (Figure 1a): (1) we horizontally sweep the focal point position of the illumination laser beam across the back focal plane of the objective from an off-axis TIRF position through the central objective position to the opposite TIRF position, and (2) we mount a tilted top mirror above the sample to back-reflect the illumination light, thus creating a near-vertical interference illumination pattern. As will be shown below, using a slight tilt of the mirror provides a means for self-calibration of IBIS.

Typically, for a sample we use a single standard glass slide onto which labels or particles of interest are deposited. A few micrometers above this sample, we mount the reflecting mirror under a slight angle α (see Materials and Methods). Light passing through the sample plane reflects on the mirror and subsequently self-interferes. To a first approximation, this causes a near-vertical standing wave pattern: a highly modulated illumination field in the z-direction that depends on the distance to the mirror (Figure 1a). This effect has been used in FLIC microscopy for height measurements close to a reflecting surface[4−6,9] and for SMI using a nontilted back-reflecting mirror.[7] Typically, an intensity modulation depth in excess of 90% occurs over a distance of order $\lambda_{exc}/2n$, where λ_{exc} is the wavelength of the incident light and n is the refractive index of the ambient medium (typically water).[4] For an aqueous sample excited with a 532 nm excitation laser and normal incidence on the mirror, an interference period of 200 nm is expected. As a consequence, the visibility of a fluorescent particle will sensitively depend on its distance from the mirror.

IBIS Modulation. Next, we alter the periodicity of the interference pattern by horizontally translating the position of the incoming beam within the back focal plane of the objective. This causes two effects:

(1) The translation ε sweeps the incoming angle θ_g (calibrated as described in Materials and Methods) of the illumination beam from one TIRF angle through coaxial epi-illumination to "opposite" TIRF (where the optical path is inverted from the initial TIRF, because the incoming beam enters at the opposite side of the objective back focal plane), see Figure 1a. For angles smaller than the TIRF angle, the light will be transmitted and refracted through the sample-surface interface and hit the mirror at an angle θ_i, defined as the incidence angle from the mirror normal. The refraction causes the angle θ_i to increase relative to θ_g such that during the translation, the light may hit the mirror at angles θ_i ranging over

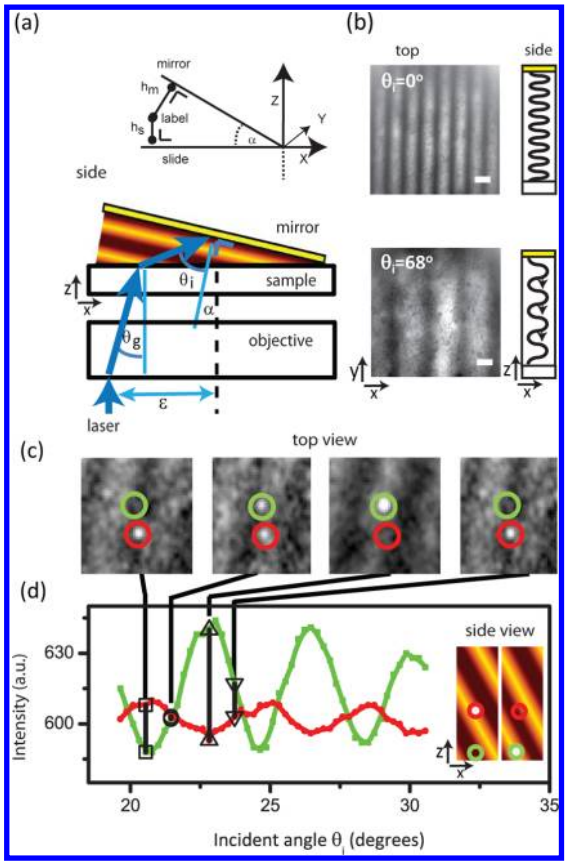

Figure 1. Measurement principle of IBIS. (a) Side view of illumination from the bottom in combination with a tilted top mirror creates a standing illumination wave (colored stripes) projected on a sample surface. Some parameters used in the main text are shown. (b) Fluorescence images of labeled proteins on sample surface, showing the surface-projected expanding wave pattern for two angles-of-incidence θ_i of the illuminating laser; scale bars 10 μm. The cartoons on the right show the relation to the vertical wave pattern; the expansion of the pattern (bottom cartoon) is schematized by arrows. (c) Snapshots of two fluorescent beads (red and green circles) suspended in an agarose gel, just above a fluorescent surface. The passing of an illumination wave causes alternating visibility of the beads. (d) Fluorescent emission as a function of illumination angle of incidence for the two beads in (c), showing strong out-of-phase modulation. Inset: side view cartoon (not to scale) of the associated bead geometry with the interference waves passing by (colored stripes).

$(180 - \alpha)°$. As shown in Supporting Information SI-1, a simple relation exists between angle θ_i and laser position ε that can be readily calibrated.

(2) An interference shift: when the mirror incident angle θ_i increases, the interference spacing will increase for the near-vertical, standing illumination pattern, scaling with $1/\cos(\theta_i)$ (see below). In other words, the interference pattern expands perpendicular to the mirror (Figure 1b, cartoons). As a consequence, any fluorescent particle away from the mirror will experience the passing of illumination maxima and minima upon the sweeping. The pattern illumination can be observed directly on the opposing glass sample surface, which was labeled with fluorescent BSA-Alexa555 for this purpose; the small tilt of the top mirror converts the near-vertical interference pattern into a projected, horizontal surface wave (Figure 1b). The original spacing λ_0 of the interference pattern will be amplified with a factor $1/\sin(\alpha)$ on the surface

projection, resulting in a surface wavelength λ_{surf} on the order of 10 μm, which is readily resolvable optically. The top panel of Figure 1b shows the surface pattern at near-coaxial illumination, or $\theta_i = 0$, where the pattern is densest, while the bottom panel shows a much more expanded pattern at a higher incidence angle of $\theta_i = 68°$. For the surface projection, the beam sweeping causes the projected wave to expand starting from the contact point, where the mirror touches the sample surface. As a consequence, both for a particle suspended in the wedgelike volume and for any location on the sample surface the induced sweep expansion of the wave pattern causes a continuous shift of the waves maxima; see also Supporting Information, Movies 1 and 2.

Our IBIS geometry allows us to employ a sideways, and thus easily feasible, translation of a laser beam to induce a near-vertical scanning modulation without a need for axial motion of the objective or the back-reflecting mirror. In the following section, we show how this modulation is used for height measurements.

Height Dependence in IBIS. The brightness of a particle's emitted fluorescent emission during the illumination sweeping depends very sensitively on its distance to the mirror surface. This is shown directly in Figure 1c,d, where we suspended small (20 nm) fluorescently labeled beads in a 2% agarose gel at random heights above a surface labeled with fluorescent BSA-Alexa555. As the incident angle θ_i is varied, microscope snapshots show the surface wave passing (Figure 1c). The red and green circles highlight two suspended particles. In Figure 1d, the corresponding two emission curves are shown; strikingly, they run strongly out of phase. Because these two particular spots are aligned parallel to the waves of the surface pattern, only a height difference can account for their phase difference (Figure 1d, inset). In addition, we note the strong height sensitivity at these intermediate angles around $\theta_i \sim 25°$: with a mere ~2° change of mirror incidence angle θ_i, a corresponding shift of half an interference spacing (i.e., ~100 nm) results in the particles switching from full to zero visibility, as can be seen in the striking variation of intensity in the green and red circles of Figure 1c; see also Supporting Information, SI Movie 3.

Quantifying Height: Model for Fluorescence Emission. For quantified height measurements, we developed two approaches: (i) an absolute "deep-sample penetration" approach where we measure any depth over many microns from a top-mounted mirror with a few tens of nanometer resolution (defined as the standard deviation of the obtained depths), and (ii) a relative method where we measure the height nearby the sample surface with 3 nm precision.

We first describe the underlying optical principle. Figure 2a provides a typical example of the semiperiodic emission of one single surface location (with average background subtracted) plotted against the angle of incidence θ_i on the mirror. A simple descriptive model for the emission of a particle at some distance from the mirror, as a function of the laser incident angle θ_i, as adapted from refs 4 and 6 (see also Supporting Information SI-1) is given by

$$I(\theta_i) \propto \sin^2\left(\frac{2\pi n \cos(\theta_i)}{\lambda_{exc}} h_m\right) \quad (1)$$

where n is the refractive index of the water, λ_{exc} is the excitation laser wavelength, and h_m is the perpendicular distance, or "depth" from the mirror, that is, distance from the mirror plane,

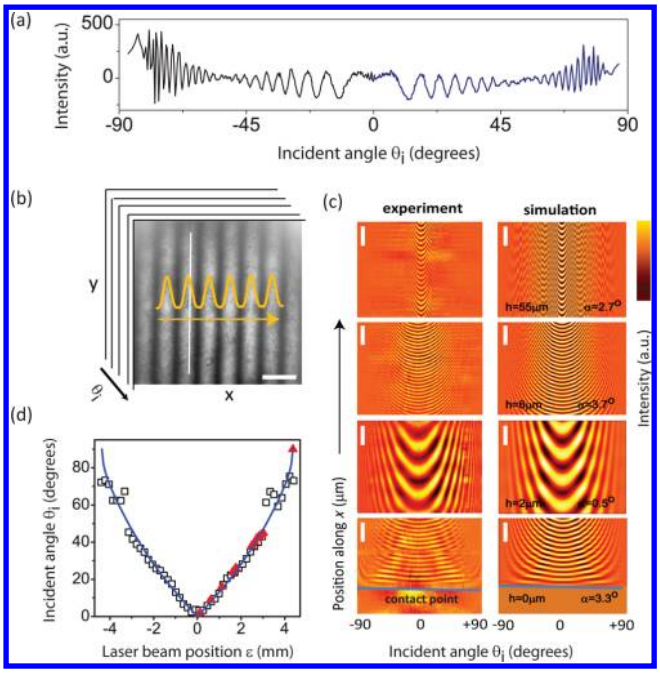

Figure 2. Surface sweep maps. (a) Example of a fluorescence emission curve of a single spot as a function of laser incidence angle θ_i. (b) Surface pattern for an intermediate laser incidence angle. Yellow curves indicate the averaged surface profile along x; scale bar 16 μm. (c) Experimental (left) and simulated (right) surface wave maps for a range of geometries (height h = 0−55 μm; mirror angle α = 0.5−3.7°); scale bars indicate a distance along the x-position axis of 16 μm. (d) Mapping of incidence angles calculated from different surface wave scans (black data points) compared to manual exit-angle measurement (red data points). The solid blue line is used as the position-to-angle calibration curve.

which is defined as $h_m = 0$. This expression is based on simple reflection interference under an angle θ_i. For the projected pattern on the surface, eq 1 simply rescales with the mirror tilt angle, α, as

$$I(\theta_i) \propto \sin^2\left(\frac{2\pi n \cos(\theta_i)}{\lambda_{exc}} x_s \sin(\alpha)\right) \quad (2)$$

using a lever rule $h_m = x_s \sin(\alpha)$, where for any fluorescent particle on the sample surface x_s is an in-plane distance to the contact point of the mirror to the sample slide, as measured along the wave propagation direction. Equation 2 predicts a periodic surface pattern with a periodicity, λ_H, that depends on θ_i (which is the only parameter varied within the experiment) as given by

$$\lambda_H(\theta_i) = \frac{\lambda_{exc}}{2n \cos(\theta_i)\sin(\alpha)} \quad (3)$$

Figure 2b shows an example of such an surface pattern for a θ_i of ~0°. We can verify this model by sweeping the angle of incidence θ_i over nearly 180° while acquiring 300−800 images, similar to Figure 2b, at an acquisition rate of ~10 Hz, such that an image stack is obtained that covers all angles of incidence. For a single snapshot image of the running wave, we average the intensities along the y-direction (Figure 2b, parallel to the white line), such that we obtain an averaged intensity of the surface wave for each image, as schematized by the yellow curve. Mapping such curves for all images, we can now build experimental surface sweep maps such as those shown in Figure

dx.doi.org/10.1021/nl501434v | Nano Lett. 2014, 14, 4469−4475

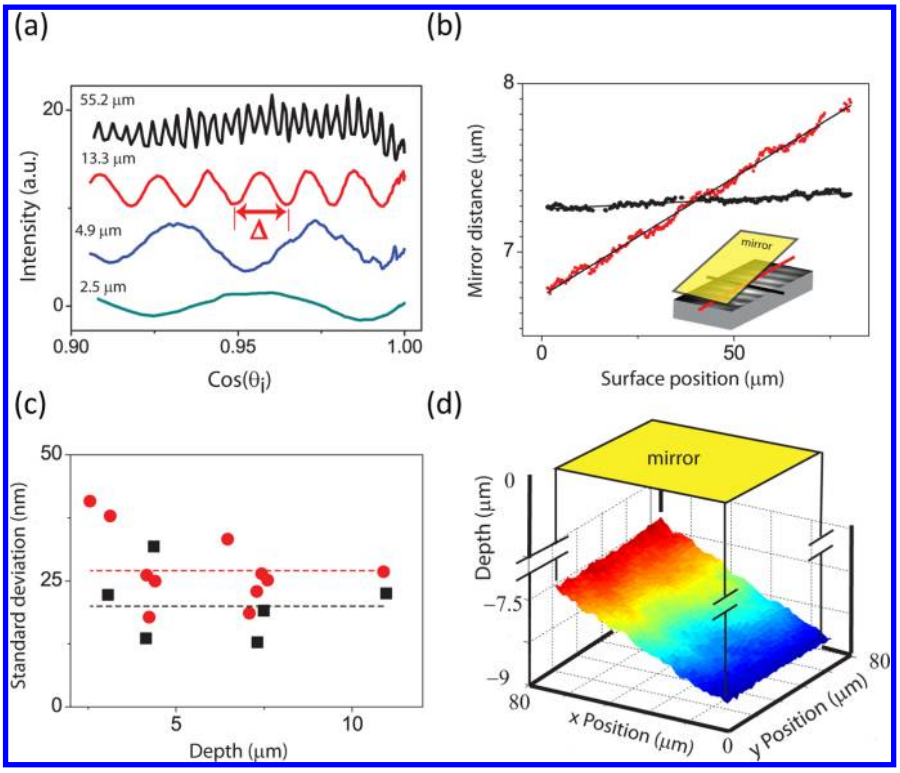

Figure 3. Deep-sample measurements. (a) Zoom-ins of emission traces of single spots plotted against the cosine of the illumination incidence angle θ_i, showing a signal with a dimensionless periodicity Δ, that scales with the distance of the fluorescent object to the mirror; calculated heights are indicated. (b) Distance from the mirror h_m of a labeled protein surface, parallel (red) and perpendicular (black) to the wave propagation direction; thin lines, linear fits. Inset: global geometry. (c) Standard deviation of height measurements for parallel (red) and perpendicular (black) surface profiles as in (b). Averages are shown as dotted lines. (d) Three-dimensional surface depth mapping of protein surface, faithfully reproducing the wedge geometry of the experiment.

2c, that display the emission intensity (in color scale) as a function of incident angle θ_i and surface position along the wave vector direction.

For a flat sample surface, the surface pattern and thus the sweep map is fully determined by the local geometry: the depth h_m as measured from the mirror and the mirror tilt angle α. Thus, using eq 2 we can calculate the surface intensity for various mirror angles α and the surface distance, or depth, from the mirror h_m. As shown in the right panels of Figure 2c, we can thus calculate the various measured surface maps along the wedge, from a midimage depth h_m of 55 μm deep (top) to the very contact point where the mirror touches the surface (bottom). The comparison of experimental results and simulations (Figure 2c) is excellent.

A quantitative check of the proposed model was performed by comparing measured and predicted incidence angles as a function of off-axis laser beam position ε (Figure 1a). As described in Supporting Information SI-1, the incident angle in the water, θ_i, as a function of ε can be measured independently (Figure 2d, red data points). In addition, eq 3 predicts that the surface sweep maps should exhibit a wavelength that scales with $1/\cos(\theta_i)$, leading to the typical arc pattern that is observed in surface sweep maps as in Figure 2c. Using eq 3, we can derive the angle of incidence as

$$\theta_i = \arccos\left(\frac{\lambda_0}{\lambda_\varepsilon}\right) \tag{4}$$

where λ_ε is the measured fringe spacing for any laser position ε, and λ_0 is the densest surface fringe spacing as encountered at $\theta_i = 0$ (in the surface sweep maps, λ_0 is represented by the midvertical cross sections). In Figure 2d, we compare the angle of incidence θ_i as calculated using eq 3 to independent exit-angle measurements for a number of surface sweep maps from different experiments ($N = 15$) using mirror tilts between 0.5 and 3°, and various locations under the mirror. Indeed, the average of the experiments (black open squares) are in excellent agreement with the exit-angle experiment (red triangles), thus confirming the validity of eqs 2−4. For the remainder of the paper, we translate laser position ε to angle of incidence θ_i using the blue solid curve in Figure 2d.

Deep-Sample Measurements. We now show that a surprisingly simple relation exists between the absolute distance of a particle from the mirror, that is, its depth h_m, and the modulation in its fluorescence emission, and that this relation holds for tens of microns deep into the sample. From inspecting eq 1, it follows that the emission of any particle is periodic as a function of the cosine of the incident angle θ_i with a dimensionless period

$$\Delta = \frac{\lambda_{exc}}{2nh_m}$$

which is inversely proportional to its depth h_m. It follows that this depth

$$h_m = \frac{\lambda_{exc}}{2n\Delta} \tag{5}$$

can be directly determined by measuring Δ, independent of the amplitude of the fluorescence emission. We determine the

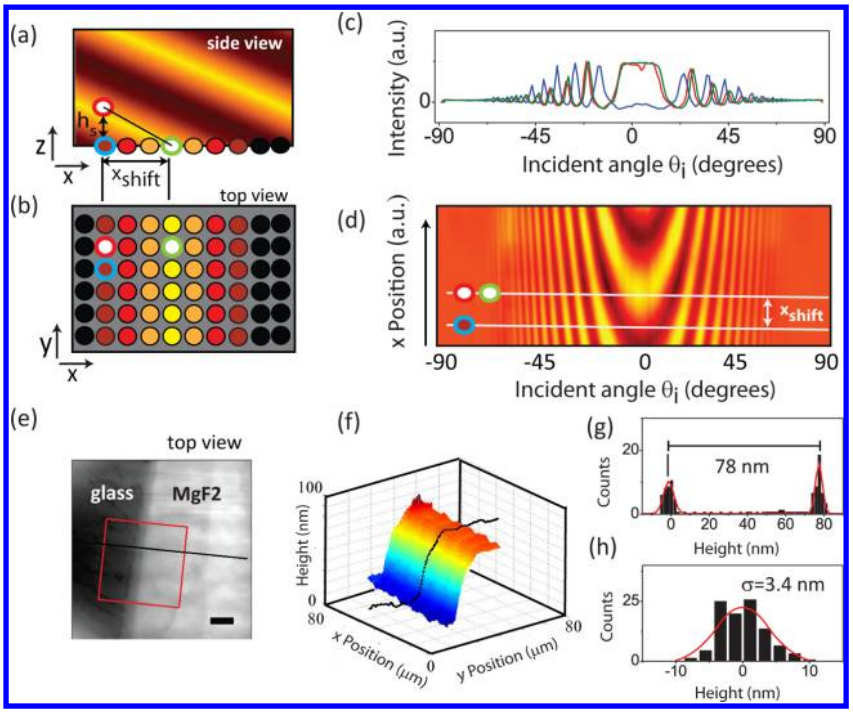

Figure 4. High-resolution relative height measurements. (a) Side view of an elevated particle (white circle with red border) in phase with a surface particle some distance x_{shift} away (white circle with green border) but out of phase with immediate neighbors underneath (red circle with blue border). (b) Same situation as in (a), now seen from above. (c) Corresponding emission curves from particles in (a), elevated (red curve) and on surface (blue and green curves). (d) Lookup-table of averaged surface emission as a function of incident angle with representative x-positions for the example particles in (a−c) indicated by white lines. A suspended particle (red) at finite height and on an x-position indicated by the lower line, may match best a surface emission (green) that is somewhat shifted (upper line). (e) Time-averaged fluorescence image of a stepped sample, consisting of a fluorescent protein layer deposited over an MgF_2 step edge; scale bar 10 μm. (f) Height mapping of a selected line (black) and area (red box) yields the three-dimensional topography of the step. (g) Height histogram of the line profile in (f) reflects the height of the step edge as 77.6 ± 0.3 nm. (h) Similar results for a nearly flat protein layer showing an upper limit of the height variation, including a measurement error (standard deviation) of only 3.4 nm.

average spacing, Δ, by autocorrelation, and the depth h_m then follows from eq 5. Examples of such periodic curves and the accompanying depths are shown in Figure 3a. We note that the limited acquisition rate will cause the sweeps to exhibit under-sampling effects at high angles, as can be clearly seen from the sweep maps in Figure 2C. To avoid this under-sampling influencing the IBIS measurement, we typically select an angular sweep range of ±45°, which is sufficient for the heights discussed in this study (0−12 μm); see also the Supporting Information, Section SI-2.3. In Figure 3b, we show the measured depths for two rows of surface points of a surface labeled with fluorescent BSA-Alexa555: one row perpendicular to the mirror tilt direction, that is, parallel to the optical interference pattern and therefore all at identical distance to the mirror (black) and one row in parallel to the tilt direction, thus at a linearly varying distance from the mirror (red). Subtracting the average slope and ignoring the local topography of the protein layer itself that includes the layer roughness of ∼2 nm, we can estimate the "perpendicular" and "parallel" resolution, defined as the standard deviation of the expected height. Figure 3c presents the result for a number of experiments at different distances from the mirror, with the "perpendicular" resolution in black and "parallel" in red. We find that over a range of 11 μm the resolution range is 10−40 nm with averages of 20 ± 3 nm (N = 6) for the perpendicular direction and 27 ± 3 nm (N = 11) for the parallel direction. In Figure 3d, a full mapping of the protein surface was performed. In this measurement, we clearly observe the tilt of the sample surface relative to the mirror. As will be explained below, this resolution can be greatly improved via a relative, sample-surface-based approach. However, the value of the present absolute method is that it can be performed over a distance from the mirror in excess of 10 μm and a precision of tens of nanometers (Figure 3c, dashed line). Such a long-range makes this approach of particular use for nonsurface applications, such as live cell imaging or gel-based particle analysis.

High-Precision Height Mapping. In many near-surface applications, measuring an absolute depth of many microns is less important than an accurate relative measurement, for example, of nearby particles relative to each other, or of a single moving particle at different time points. Here we show that we can also use the sweep maps introduced in Figure 2c as "look-up-tables" (LUTs) to perform high-precision local height measurements. To do so, we first consider the geometry shown in Figure 4a. While an elevated particle is out of phase with particles directly underneath it (red and blue circles), it will be in phase, that is, exhibiting similar emission curves, with particles that are located at the surface at a distance x_{shift} to the right as shown in the depicted geometry (green circle). In Figure 4b, the associated top view is shown, similar to the experimental case in Figure 1c,d. At these very shallow angles, the relation between "surface height" h_s (perpendicular to the sample surface) and x_{shift} can subsequently be described by a simple lever rule

$$h_s = x_{shift} \tan(\alpha) \tag{6}$$

dx.doi.org/10.1021/nl501434v | Nano Lett. 2014, 14, 4469−4475

with

$$\alpha = \arcsin\left(\frac{\lambda_V}{\lambda_H}\right)$$

where λ_V is the interference spacing perpendicular to the mirror, λ_H is the associated surface projected spacing, and α is the mirror tilt angle (see also Supporting Information, Figure SI-1b) . While both λ_H and λ_V vary during a scan, their ratio is constant. Experimentally, α is easily found via

$$\alpha = \arcsin\left(\frac{\lambda_{exc}}{2n\lambda_0}\right) \tag{7}$$

where λ_0 is the densest surface spacing observed at $\theta_i = 0$. A relative height measurement amounts to finding the shift x_{shift} between the particle or label of interest and those surface particles that emit identical in-phase emission curves, as depicted schematically in Figure 4b. To do this, we should match emission curves as shown in Figure 4c. Since a surface sweep map, as shown in Figure 4d, is simply a collection of all possible averaged emission curves at the surface, we can use it as a LUT for the emission of our particle of interest. To do so, we follow a standard error minimization routine, using the summed χ^2 difference of a particle of interest's emission curve with every emission curve in the LUT. The resulting error curve, as a function of position along x, will show a series of minima and we select the minimum closest to the actual position, x_p, of the spot. The precise position of this minimum, x_{min}, is refined by subpixel parabola fitting. Finally, $x_{shift} = |x_p - x_{min}|$ and the height, h_s, can be determined using eq 6.

In Figure 4e,f, we demonstrate the technique by mapping a prefabricated transparent step of known height, which was made from low-refractive index MgF_2 to eliminate optical aberrations. Both levels of the step were coated with fluorescent BSA-Alexa555. In Figure 4e, the mean fluorescence intensity (averaged over many periods of the sweeping surface wave) is depicted. We sampled a dense grid and a line scan perpendicular to the propagation vector of the wave (Figure 4e, red box and black line, respectively). Figure 4f shows the measured topography of the square grid and the line scan with the histogram of the line scan data shown in Figure 4g. After peak fitting of the histogram, we find a height of the MgF_2 edge of 77.6 ± 0.3 nm, which is in excellent agreement with the 76 ± 3 nm layer thickness that was measured by ellipsometry.

Figure 4h shows a histogram of a similar height measurement from a line scan on a saturated BSA-Alexa555 layer on a glass surface. Again, we selected a box for height mapping of the surface and a line scan perpendicular to the wave propagation to evaluate the resolution. In a perpendicular line scan profile, we observe a standard deviation of only 3.4 nm. We note that this standard deviation encompasses both the IBIS measurement error and height variations due to the true topography, so that the actual IBIS resolution likely is even better.

In this paper, we have described a new technique, IBIS, which is a capable of measuring relative heights of fluorescent surfaces and particles with nanoscale resolution without strong requirements on sample conditions or microscope modifications. IBIS can be applied in two modes:

(1) A long-range approach with a precision of a few tens of nanometers over a range greater than 10 μm, offering the possibility to measure in micrometer-sized volumes such as in living cells with specifically labeled proteins, or along vertically stretched DNA tethers as commonly used in magnetic tweezers experiments.[12] From IBIS simulations on simulated traces with increasing levels of noise, we infer that the main limiting factor to IBIS resolution is the noise in the fluorescent traces (Supporting Information, Section SI-2).

(2) A second approach offers high precision (likely better than 3 nm) in a range limited by the periodicity of the employed interference pattern in this case about 200 nm. This is particularly useful for applications with a limited height range, such as surface- or membrane-related processes, or for following diffusion in confined spaces in 3D.

Because IBIS is based on standard microscopic imaging, the heights of any point in the field of view can be acquired in parallel. IBIS works equally well for image mapping, where every pixel point is analyzed in parallel, as for spot-detection, where individual, optically separated particles are detected. IBIS is also compatible with multicolor fluorescence experiments, because calibration only depends on the properties of the illumination field.

Our current best resolution is 3.4 nm, as measured on static, flat protein surfaces. Because we cannot rule out a contribution of surface roughness in this best result, the potential precision might be even higher. As for temporal resolution, while our current measurements were acquired in a 30 s time window, thus presenting an effective bandwidth of 1/30 Hz for determining the position of a particle, IBIS can be easily advanced to track dynamic particles; the lateral beam sweep rate can be made much faster (~1000 Hz) by use of, for example, piezo mirrors, such that the limiting factor is ultimately the camera acquisition rate and the number of sampling points (images) needed to define a phase difference. We estimate that an ~100 Hz bandwidth should be possible. IBIS is fully compatible with standard in-plane localization and thus simultaneously allows a lateral (x,y) resolution from point spread function (PSF)-limited fluorescent imaging of $1-10^2$ nm depending on the amount of associated labels and corresponding photons that can be measured. Ultimately, the corresponding noise level in the fluorescent traces (see Supporting Information SI-2.2) will set a minimum time window for obtaining a single height and thus a maximum bandwidth.

In general, the main requirement for applying IBIS to a broad range of biological samples is that one should work in reflection mode, not in transmission. The slight mirror tilt can be accomplished by many other simple mechanical solutions instead of involving a contact point (which for the presented measurements was the simplest approach). We further note that while for the present study the mirror was typically at a distance of 5−10 μm, the mirror can be mounted much further away and even outside a flow cell, while sweeping closer to the optical axis to avoid under-sampling (see Supporting Information, Section SI-2.3).

We conclude that IBIS provides an easy-to-implement, quantitative add-on to fluorescent epi- and TIRF-based experiments, allowing topographic mapping or 3D localization and 3D tracking of fluorescent particles inside otherwise inaccessible structures, such as living cells.

Materials and Methods. *Mirror and Sample Mounting.* For a sample, we typically use a single glass slide onto which labels or particles of interest are deposited. Above this sample, we mount a reflecting mirror by gluing a thin gold-evaporated glass slide to a 60 × 5x0.1 mm thin glass cantilever slide. This cantilever is bent toward the sample by a bridging screw until

the mirror edge makes contact, thus making a stable mirror wedge under a very shallow angle α (~1°).

Sample Preparation. Standard microscopy slides were incubated for 5 min with a solution of Alexa555-labeled BSA (Invitrogen BSA -Alexa Fluor 555) to create a homogeneous fluorescent surface layer. Fixed suspensions of (20 nm) fluorescently labeled beads were made by mixing them in a 2% low-melt agarose solution (Sigma) and pipetting this solution between mirror and protein-labeled glass slide on a 40C hot plate, after which the gel was cooled. Step samples were made by depositing a transparent MgF_2 layer with an average thickness of 76 ± 3 nm (as measured by ellipsometry) on a glass slide, creating an corresponding step edge. Prior to the measurement, the sample was incubated with fluorescently labeled BSA solution.

Beam Path. For illumination, we use a 532 nm wavelength laser beam (Coherent) of width ~1 mm that is focused onto the back focal plane of a TIRF objective (Olympus 60×, NA = 1.45) mounted on a microscope base, leading to a narrow, parallel beam entering the sample (see also Supporting Information). We shift the axial position of the incoming beam by translating a mirror and a laser beam expanding lens using a simple battery-powered actuator (Lego Inc.) driving a translation stage. Scanning the full range of accessible angles in between the two TIRF angles takes about 40 s.

Acquisition. We use an Andor iXon 897 emCCD Camera operated at 10 Hz. Custom software for analyzing images, processing emission curves, and building LUTs was written in MATLAB. Simulations as shown in Figure 2c, right panels, were written in MATLAB.

Notes. We note that in eqs 1 and 2 we ignore the effect of emission interference, that is, self-interference of the light emitted by the fluorescent particle, because we expect the coherence length of the emitted light to be much less than the typical distance to the mirror h. This is justified from inspecting the surface sweep maps: because emission is not dependent on the direction of the incidence light, emission interference would show an additional angle-independent modulation, that is, a horizontal (nonarched) modulation in the experimental surface maps, which is only faintly visible and is therefore ignored. See also Supporting Information, Section SI-1.1.

■ ASSOCIATED CONTENT

Supporting Information

SI-1: Description of IBIS geometry and definition of coordinates. **SI-2**: Study of the influence of experimental errors on IBIS resolution. **SI-3**: Discussion of IBIS applications and outlook. **Movie S1**: Example of an IBIS sweep scan over a prefabricated transparent MgF_2 step coated with fluorescent BSA-Alexa555; image size 80 μm. **Movie S2**: Example of an IBIS sweep scan over a glass slide coated with fluorescent BSA-Alexa555; image size 80 μm. The image shows the region where the tilted mirror is in contact with the glass slide. **Movie S3**: IBIS sweep scan of the experiment with suspended beads as described in Figure 1c,d. This material is available free of charge via the Internet at http://pubs.acs.org.

■ AUTHOR INFORMATION

Corresponding Author

*E-mail: c.dekker@tudelft.nl.

Author Contributions

†J.W.J.K. and T.R.B. contributed equally.

Notes

The authors declare no competing financial interest.

■ ACKNOWLEDGMENTS

This work was supported by the ERC Advanced Grant NanoforBio (No. 247072) and by The Netherlands Organisation for Scientific Research (NWO/OCW), as part of the Frontiers of Nanoscience program. T.R.B. was supported by a Marie Curie International Incoming Fellowship within the seventh European Community Framework Programme.

■ REFERENCES

(1) Quirin, S.; Pavani, S. R. P.; Piestun, R. *Proc. Natl. Acad. Sci. U.S.A.* **2012**, *109* (3), 675−679.
(2) Huang, B.; Wang, W.; Bates, M.; Zhuang, X. *Science* **2008**, *319* (5864), 810−813.
(3) McMahon, M. D.; Berglund, A. J.; Carmichael, P.; McClelland, J. J.; Liddle, J. A. *ACS Nano* **2009**, *3* (3), 609−614.
(4) Kerssemakers, J.; Howard, J.; Hess, H.; Diez, S. *Proc. Natl. Acad. Sci. U.S.A.* **2006**, *103* (43), 15812−15817.
(5) Lambacher, A.; Fromherz, P. *Appl. Phys. A: Mater. Sci. Process.* **1996**, *63* (3), 207−216.
(6) Wong, A. P.; Groves, J. T. *J. Am. Chem. Soc.* **2001**, *123* (49), 12414−12415.
(7) Mathée, H.; Wotzlaw, C.; Cremer, C.; Birk, U.; Baddeley, D. *Opt. Eng.* **2007**, *46* (8), 083603−083603−8.
(8) Reymann, J.; Baddeley, D.; Gunkel, M.; Lemmer, P.; Stadter, W.; Jegou, T.; Rippe, K.; Cremer, C.; Birk, U. *Chromosome Res.* **2008**, *16* (3), 367−382.
(9) Kerssemakers, J.; Ionov, L.; Queitsch, U.; Luna, S.; Hess, H.; Diez, S. *Small* **2009**, *5* (15), 1732−1737.
(10) Li, H.; Yen, C.-F.; Sivasankar, S. *Nano Lett.* **2012**, *12* (7), 3731−3735.
(11) Berndt, M.; Lorenz, M.; Enderlein, J.; Diez, S. *Nano Lett.* **2010**, *10* (4), 1497−1500.
(12) De Vlaminck, I.; Dekker, C. *Annu. Rev. Biophys.* **2012**, *41* (1), 453−472.